

## Magnetohydrodynamic Analysis of Load Shifting in Hall-Héroult Cells

Hendrik Gesell<sup>1</sup> and Uwe Janoske<sup>2</sup>

1. Research Associate

2. Professor

University of Wuppertal, Wuppertal, Germany

Corresponding author: gesell@uni-wuppertal.de

### Abstract

The research project SynErgie aims to adapt large scale industrial processes to a volatile supply of renewable energy which is expected for the future. The aluminium electrolysis process is one of the biggest consumers of electric energy in Germany. The aim is to vary its nominal process power by  $\pm 25\%$ . This numerical study focuses on the magnetohydrodynamic (MHD) behaviour of the electrolysis cells of Trimet Aluminium SE in Essen. To capture the MHD driven flow and electrodynamic inside the electrolysis cells a computational fluid dynamics (CFD) model is developed in the OpenFOAM® framework. This accounts for the influence of neighbouring electrolysis cells, the magnetization of ferromagnetic materials, a static ledge profile and the dynamic changes of anode shape caused by the carbon consumption. The simulation predictions show the heave of the aluminium cryolite interface for different line currents. To analyze the behaviour of flexible process operation, shifts of the line currents are studied in detail. After shifting the line current, the interface heave changes directly whereas the shape of the anode bottom reacts with a delay in time. This leads to a locally uneven anode cathode distance (ACD) followed by a disturbed current distribution inside the electrolysis cell after shifting the line current. The anodic current distribution is quantified by the model, which can help process operators to identify whether increased anode currents are caused by the line current shift or potential abnormalities like spikes.

**Keywords:** Magnetohydrodynamics, Hall-Héroult, Aluminium electrolysis, Current modulation, Metal pad heave.

### 1. Introduction

As the number of renewable electricity sources is increasing, the volatility of electric energy in the grid raises. This trend also affects large scale industrial processes, as the availability and the price of electric energy become more relevant. Trimet Aluminium SE aims to design the aluminium electrolysis pot lines flexible in terms of current input. To adapt the technology of the electrolysis cells, magnetic compensation of the cells has been installed by means of a modification to the pot busbars, which allows higher line currents and reduces problems related to cell control. Moreover, to maintain the thermal balance of the electrolysis cells, shell heat exchangers have been installed [1].

Despite of these actions, shifts of the line current still impact the process operation. These impacts and its consequences are the subject of the current study. It focuses on the operating condition after shifting the line current by  $\pm 25\%$ . The results help process operators to understand the dynamics of the electrolysis cells and to adapt their actions regarding process operation accordingly.

## 2. Physical Background

In this section, the relevant equations to describe electrodynamics, magnetic fields and the resulting fluid mechanics are described. These are the basis of the implemented solvers, which were employed to execute the current study.

The electric potential of a system without free charges can be described by:

$$\nabla \cdot (\sigma \nabla \Phi) = \nabla \cdot (\sigma (\mathbf{u} \times \mathbf{B})) \quad (1)$$

where:

- $\sigma$  Electric conductivity, S/m
- $\Phi$  Electric potential, V
- $\mathbf{u}$  Velocity, m/s
- $\mathbf{B}$  Magnetic flux density, T.

This equation implies that the current density must be divergence free. The current density can be expressed by:

$$\mathbf{J} = \sigma (-\nabla \Phi + \mathbf{u} \times \mathbf{B}) \quad (2)$$

where:

- $\mathbf{J}$  Current density, A/m<sup>2</sup>.

Both the electric potential  $\Phi$  and the current density  $\mathbf{J}$  can be divided into a velocity dependent and a velocity independent part. Ampere's Circuit Law, which denotes the relationship between current density and the magnetic flux density induced by it, can be expressed as:

$$\nabla \times \mathbf{B} = \mu_0 \mathbf{J} \quad (3)$$

where:

- $\mu_0$  Magnetic permeability of free space, H/(m).

In this study,  $\mathbf{B}$  is determined from the current density with the help of Biot-Savart Law, given by Equation (4). Note that subscripts  $r$  and  $r'$  indicate that a given parameter is evaluated at that particular spatial location (e.g.,  $\mathbf{B}_r$ ).

$$\mathbf{B}_r = \frac{\mu_0}{4\pi} \int_V \frac{J_{r'} \times (\mathbf{r} - \mathbf{r}')}{|\mathbf{r} - \mathbf{r}'|^3} dV_{r'} \quad (4)$$

where:

- $V$  Volume, m<sup>3</sup>
- $r'$  Location of current source, m
- $r$  Location of evaluation point, m.

$\mathbf{B}$  is related to magnetic vector potential by:

$$\mathbf{B} = \nabla \times \mathbf{A} \quad (5)$$

where:

- $\mathbf{A}$  Magnetic vector potential, V s/m.

Combining Equations (4) and (5), the magnetic vector potential can be written as:

$$\mathbf{A}_r = \frac{\mu_0}{4\pi} \int_V \frac{\mathbf{J}_{r'}}{|\mathbf{r}-\mathbf{r}'|} dV_{r'} \quad (6)$$

Equation (6) is discretized and then solved as a volume integral at the boundaries for the magnetic vector potential  $\mathbf{A}$  with the help of the Barnes-Hut method [2], which is grouping grid cells into different nodes in an octree structure. The advantage of this procedure is that only the contribution of nearby grid cells has to be calculated directly. Grid cells with a far distance are approximated as large groups. This clearly reduces the numerical efforts. Solving Biot-Savart Law directly would result in a number of computations of  $O(N^2)$ , with  $N$  as the number of grid cells. With the help of the Barnes-Hut method this can be reduced to a number of computations of  $O(N_B \log(N))$ , with  $N_B$  as the number of boundary faces. The described method allows a computation of  $\mathbf{A}$  without adding a surrounding volume of air saving a lot of computational efforts. Boundaries are all outer surfaces of the different electrolysis cell components. The internal values of the magnetic vector potential  $\mathbf{A}$  can be determined by combining Equations (3) and (5), leading to  $-\nabla^2 A = \mu_0 \mathbf{J}$ .

For the cases where ferromagnetic materials are considered, the magnetic flux density is the sum of two contributions  $\mathbf{B} = \mathbf{B}_I + \mathbf{B}_M$ , where subscript <sub>I</sub> relates to current and <sub>M</sub>, to magnetization. [3]. The magnetic vector potential is then calculated as:

$$\mathbf{A}_r = \frac{\mu_0}{4\pi} \int_V \frac{\mathbf{J}_r + \nabla \times \mathbf{M}_{r'}}{|\mathbf{r}-\mathbf{r}'|} dV_{r'} \quad (7)$$

where:

$\mathbf{M}$  Magnetization matrix, A/m.

This equation can be split into a free part including free currents  $\mathbf{J}_r$  and a bounded part including the magnetization  $\nabla \times \mathbf{M}_{r'}$ . The magnetization matrix can be written as:

$$\mathbf{M} = \mathbf{H}(\mu_r - 1) \quad (8)$$

where:

$\mathbf{H}$  Magnetic field strength, A/m

$\mu_r$  Relative magnetic permeability, dimensionless.

Finally, total magnetic flux density  $\mathbf{B}$  (*i.e.*, both contributions  $\mathbf{B}_I + \mathbf{B}_M$ ) is calculated according to Equation (5).

The source for acceleration of the fluid phases is the Lorentz Force, defined by:

$$\mathbf{F}_L = \mathbf{J} \times \mathbf{B} \quad (9)$$

where:

$\mathbf{F}_L$  Lorentz Force, N/m<sup>3</sup>.

The governing equations to describe the fluid flow for MHD problems are presented next. The velocity and pressure fields of the incompressible fluids are obtained by the momentum equation expressed by:

$$\rho \frac{\partial \mathbf{u}}{\partial t} + \rho(\mathbf{u} \cdot \nabla)\mathbf{u} = -\nabla p + \mu \nabla^2 \mathbf{u} + \mathbf{F}_L \quad (10)$$

where:

t Time, s

$\rho$  Density, kg/m<sup>3</sup>  
 $p$  Pressure, Pa  
 $\mu$  Dynamic viscosity, Pa s.

Surface tension is neglected. The continuity equation ensures the conservation of mass. For incompressible fluids it is:

$$\nabla \cdot \mathbf{u} = 0 \quad (11)$$

To capture both fluids arising in Hall-Héroult cells, the volume of fluid (VOF) approach is utilized. Therein, the momentum equation is only solved once for all fluids. To differentiate the fluids  $\alpha$  is used as a phase fraction variable. It is updated every timestep with the help of the following equation:

$$\frac{\partial \alpha}{\partial t} + \nabla \cdot (\mathbf{u} \alpha) = 0 \quad (12)$$

where:

$\alpha$  Phase fraction, dimensionless.

### 3. Numerical Model

The physics described above is implemented in the OpenFoam® framework (version 7). This framework is based on the Finite Volume Method and is implemented in C++ language. The basis of the currently employed algorithms was developed by [4].

The global workflow for this study is presented in Figure 1. The first step is to calculate a static current distribution within the electrolysis cell while ignoring fluid motion. In this step the neighbouring electrolysis cells are considered. This current distribution is then mapped into the next simulation (second step), which determines the magnetization of the ferromagnetic materials. The magnetized material influences the magnetic fields in the electrolysis cells. Here, the potshell is magnetized. The result of this step is  $\mathbf{B}$  distribution which is applied as external magnetic flux density to the MHD simulations, the third step, including the prediction of the consumed anode profile in steady-state operating conditions. The resulting anode profile is the basis for the last analysis step.

As the situation directly after shifting the line current is computed, the anode shape obtained from step three is kept constant (or “frozen”), and the MHD behaviour is solved anew. The outputs of this step, especially the anodic current distribution, will be the focus of this study.

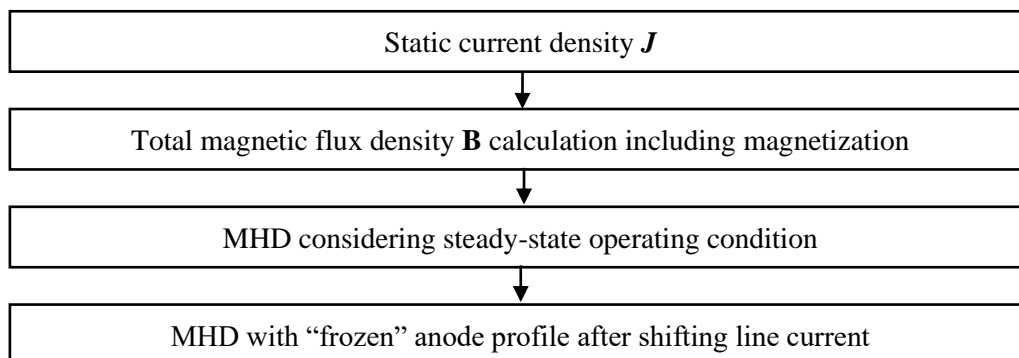


Figure 1. Global analysis workflow to simulate the MHD behaviour of electrolysis cells.

### 3.1 Anode Consumption

The dynamic anode consumption model is based on the following assumption: the interface between aluminium and bath bulges due to action of electromagnetic forces (heave). The anodes blocks, consisting of carbon, are permanently consumed according to the alumina reduction equation. The local anode-cathode distance (ACD) is assumed uniform in the whole electrolysis cell, as this balances out the ohmic voltage drop of the electrolytic bath. As a result, the bottom surface of the anodes blocks has necessarily to conform to the resulting metal pad-bath interface. Similar anode shape is reported by [5].

This mechanism is implemented in the numerical model in the same way as it is described above. The simulation has ACD as boundary condition and local anode height is adjusted to match it. All grid cells corresponding to the anode blocks are marked with the attribute “anode” by the solver and their electric conductivity is set accordingly. This is done every timestep until convergence of the numerical model is reached.

The resulting profiles from that model have an increased current density at the corners of the carbon blocks. As an increased current density also means more carbon consumption, the carbon at these locations is consumed faster. This leads to rounded anodes edges. This mechanism is also respected by the model. For this, the model removes said “anode” attribute of all grid cells which have a current density above a given threshold. Figure 2 shows a photograph of an anode which was removed from an electrolysis cell and the corresponding predicted shape by the numerical model.

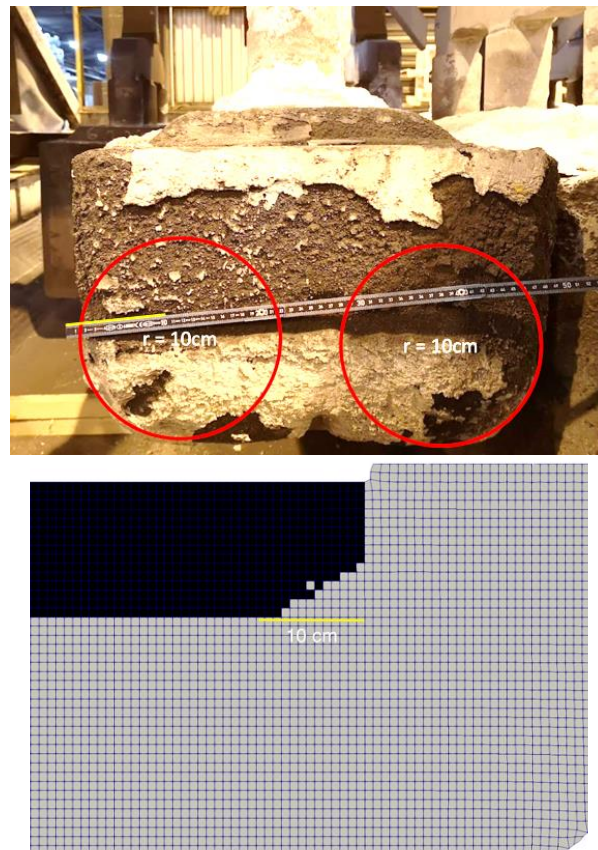


**Figure 2. Anode block with rounded corners. Top: photograph from industrial anode block, Bottom: numerical prediction.**

### 3.2 Electrolysis Cell Geometry at Trimet

The simulations are executed using electrolysis cells of the type EPT14, which are installed in two reduction halls at Trimet in Essen. The electrolysis cells are designed in an end-to-end fashion and have originally been planned for a line current of 140 kA. Now, the electrolysis cells are able to cope with higher line currents as they have been upgraded in terms of both magnetic and thermal behavior [1][6].

Figure 3 shows the numerical grid for the cell of interest consisting of 15 regions. Here, regions mean all components of the electrolysis cells like steel shell, busbars, anodes, cathode and lining materials. The adjacent electrolysis cells are considered by the Burnes-Hut algorithm using tree-structured division of geometry into cubic cells [2]. In this study three cells are considered in the upstream and downstream direction, respectively. Moreover, the opposite side in the same potroom is also included with the same amount of electrolysis cells plus the direct opposite electrolysis cell. This results in 13 neighbouring electrolysis cells taken into account.

The authors are aware that, by not considering the neighboring rows of pots in their entirety leads some error of the bias of the vertical component of the magnetic flux density  $\Delta B_z$ , leading to some error of the velocity distribution in the metal. Nevertheless, given that the metal pad heave is mostly dependent on the divergence of the horizontal components of the Lorentz forces  $\nabla \cdot F_{L,XY}$ , it is rationalized that the absence of the (mostly) uniform contribution of  $\Delta B_z$  should not considerably impact the prediction of the metal pad heave.

The mesh consists of 15.3 million grid cells which are mostly hexahedral. The inlet and outlet for  $\mathbf{J}$  are applied on the downstream and upstream ends of the busbar system as outlined. The outer boundaries of the simulation domain have Neumann boundary conditions. The gradient of  $\mathbf{J}$  is zero, which means that the current cannot pass these boundaries. The internal boundaries between the different regions are coupled to those of their neighbours. The current distribution inside the electrolysis cell is dominated by the electric conductivities of the individual components.

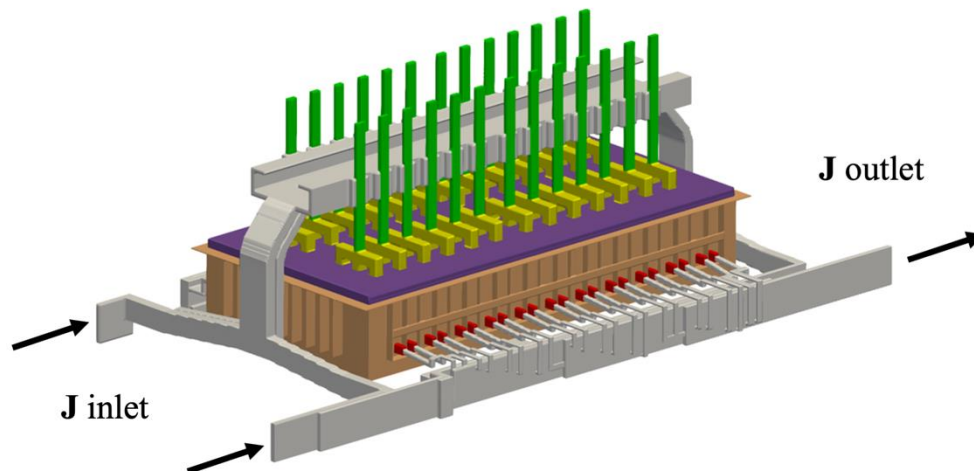
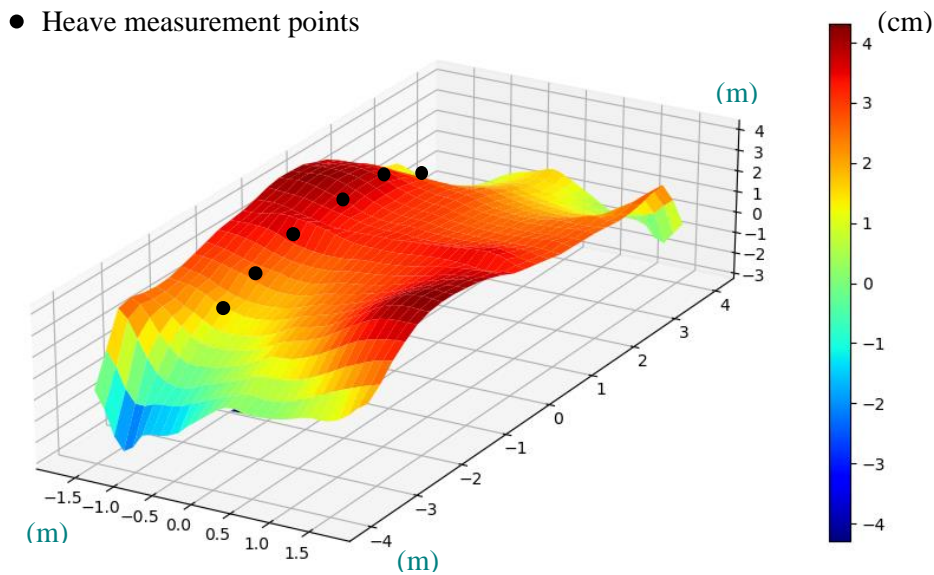


Figure 3. Simulation domain for the cell of interest (other considered conductors not shown).

## 4. Results

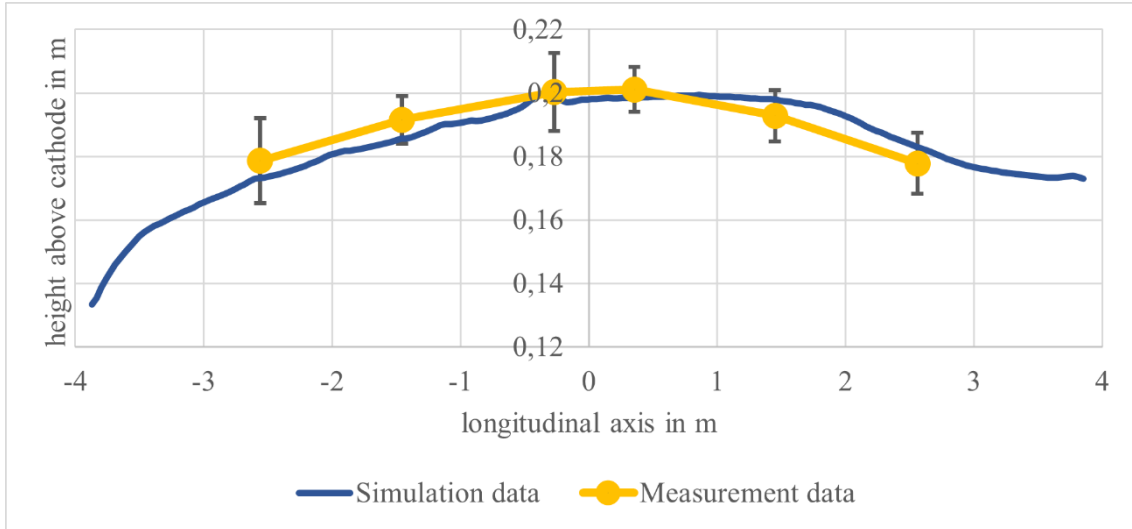
### 4.1 Standard Operation at 165 kA and Validation of Simulation Results

Nowadays, the EPT14 electrolysis cells are operated with a line current of 165 kA, which is the standard operating condition. The first simulation treats this situation. The resulting interface heave is presented in Figure 4. The total metal upheaval is approximately 8 cm and there are two positions of highest heave at both long outsides. These are  $-2\text{ m}$  and  $1\text{ m}$  away from the cell center. According to the assumption described in section 3.1, the anode bottom surfaces conform to this shape, resulting in a uniform local ACD.



**Figure 4. 3D bath-aluminium interface in EPT14 electrolysis cell at 165 kA line current.**

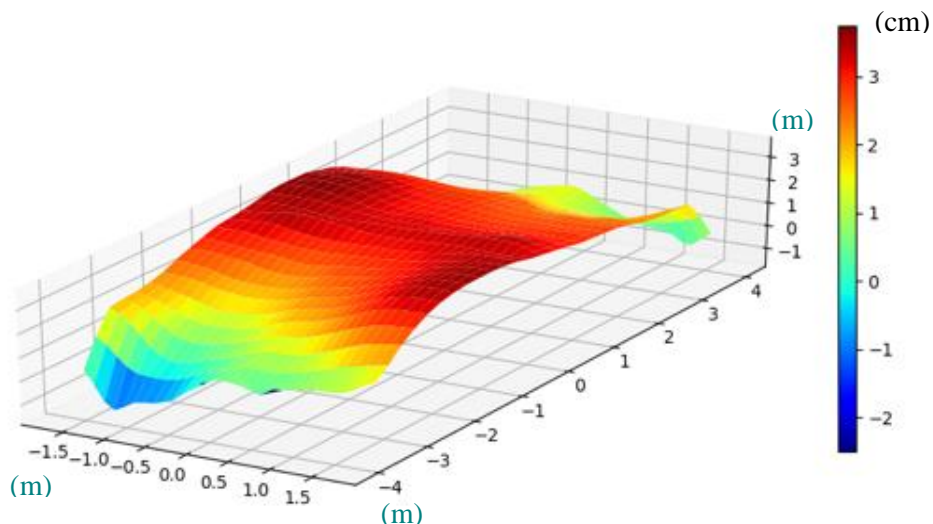
The data which has been generated with the help of the simulations is validated using measurement data from the electrolysis process at Trimet in Essen. The interface height was measured at six different positions in the electrolysis cells from the side facing outside of the potline – refer to Figure 4. To allow for the measurements, the crust was broken between the anodes. The distance to the interface was determined using steel rods. As a consistent vertical reference, the horizontal bar holding the anodes was selected. The measurements were executed in February 2022 at six different electrolysis cells. The results are presented in Figure 5. The plot shows the average values from all electrolysis cells considered in the measurements and the simulation data. A good agreement between simulation data and measurements can be seen.



**Figure 5. Validation of bath-aluminium interface in EPT14 electrolysis cell at 165 kA. The error bars represent the standard deviation.**

#### 4.2 Line Current Shifting by $\pm 25\%$

The standard operating condition described before is shifted to a 25 % higher and lower line current in the next step. This means, that the new line currents of 124 kA and 206 kA cause a new interface shape directly after shifting the line current. The interface shapes after shifting the line current can be observed in Figure 6. Decreasing the line current leads to a smoother interface shape and increasing leads to an accentuation of local maxima of the interface. As expected, the maximum metal upheaval decreases at lower line current (5 cm at 124 kA) and increases at higher load (11 cm at 206 kA).



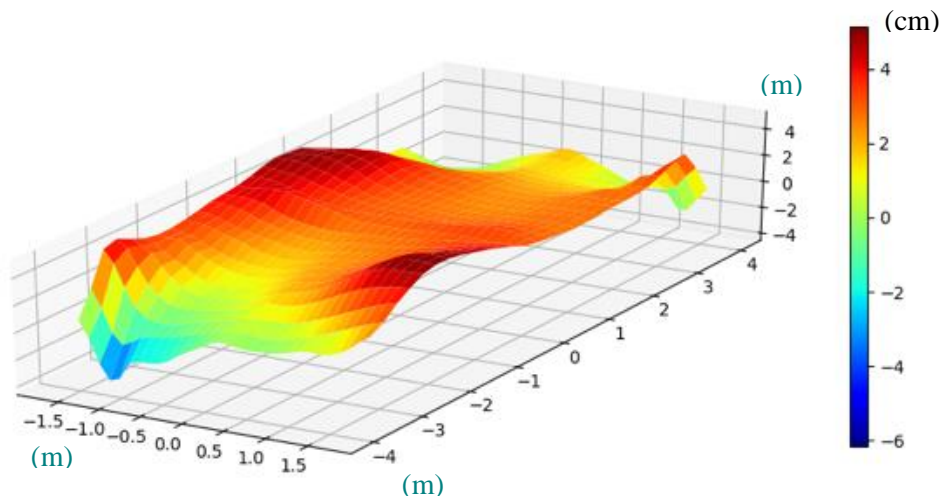


**Figure 6. 3D Cryolite-aluminium interface, in EPT14 electrolysis cell immediately after line current shifting from 165 kA. Top: 124 kA, Bottom: 206 kA.**

The anode currents are permanently monitored in some electrolysis cells at Trimet in Essen. This can help to identify process abnormalities like spikes [7]. Figure 7 presents the individual anode currents after a shift of the line currents. There are mainly two regions in the electrolysis cell, which have increased anode currents immediately after increasing current by 25 %. The regions correspond to the maxima in the interface bulge presented in Figure 4. They cause an increase of the individual anode currents up to + 10 % compared to the average (nominal) anode current.

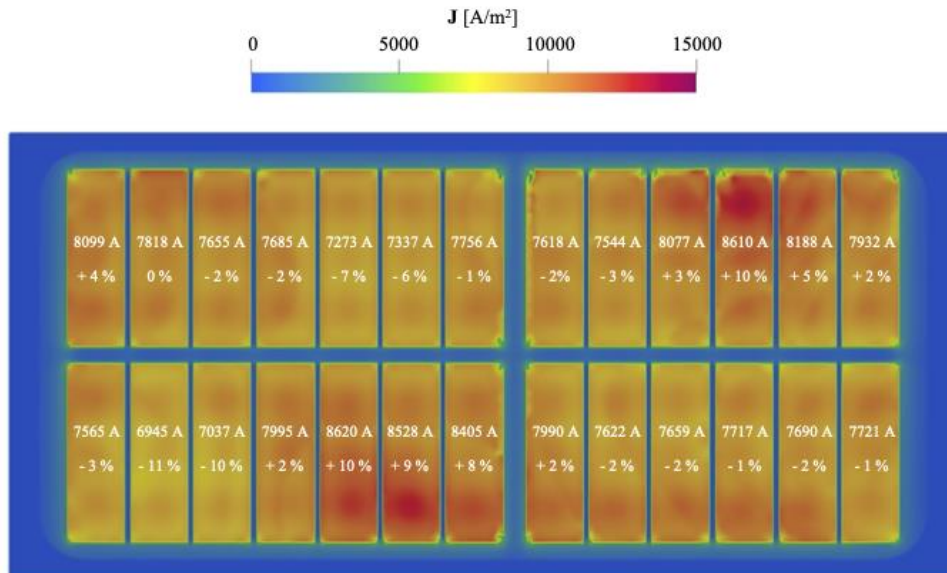


**Figure 7. Current distribution in the anodes after shifting the line current from 165 kA to 206 kA. The percentages show the deviation from the average (nominal) anode current.**

Figure 8 presents the individual anode currents after a decrease of the line current to 124 kA. The individual anode currents tend to increase at the corner anodes due to the flattening of the interface. That leads to increased anode currents up to 16 % compared to the average line current. The two regions with the highest heave at 165 kA and 206 kA have decreased anode currents also

due to the flattening of the interface. All in all, the situation at 124 kA is by tendency the opposite to the situation of 206 kA.

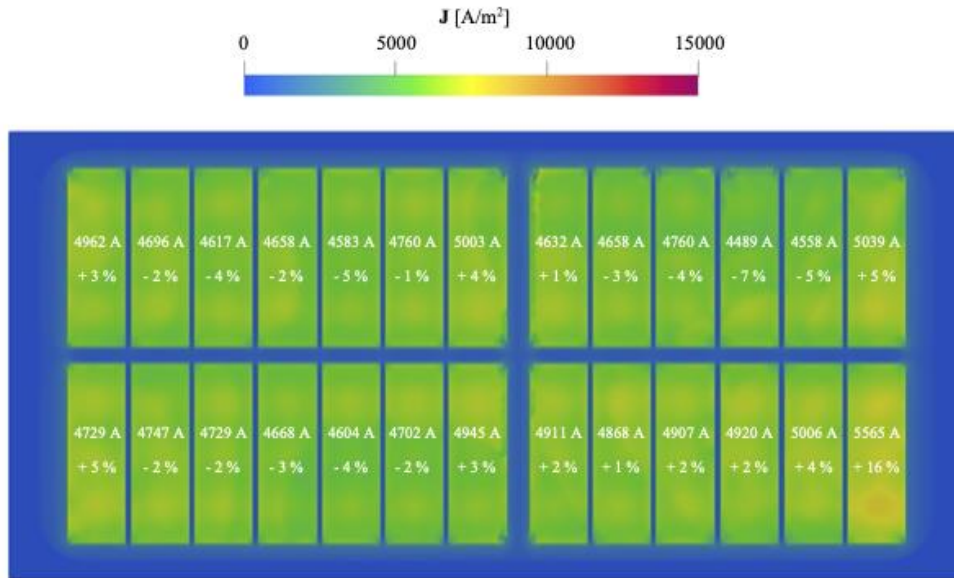


**Figure 8. Current distribution in the anodes after shifting the line current from 165 kA to 124 kA. The percentages show the deviation from the average (nominal) anode current.**

## 5. Conclusion

In the present numerical study, our MHD model for the simulation of Hall-Héroult cells is presented and applied to industrial EPT14 cells used at Trimet in Essen. The focus of the study is to analyze load shifting scenarios occurring at flexible operating conditions of aluminium electrolysis. The motivation for current modulation is to adapt industrial processes to a volatile supply of renewable electricity sources. The numerical model is able to consider the influence of neighbouring electrolysis cells, the magnetization of ferromagnetic materials, a static ledge profile and the dynamic changes of anode shape caused by the carbon consumption. Two load shifting scenarios are studied in detail. The standard line current of 165 kA is shifted to 124 kA and 206 kA which corresponds to a 25 % decrease or increase. The model predicts a flatter aluminium cryolite interface during the decreased line current situation. Combined with the anode bottom shape which was formed at the standard operation of 165 kA, this situation leads to relatively increased anode current at the corner anodes of up to 16 %. After increasing the line current to 206 kA, the interface deformation is reinforced, which leads to an increase of local current density maxima. Certain anodes have up to 10 % higher currents compared to the average anode current.

## Acknowledgements

This research is financed by the *Bundesministerium für Bildung und Forschung* under the project SynErgie II (03SFK3B1-2), whose support is gratefully acknowledged by the authors.

## 6. References

1. Roman Düssel, Albert Mulder and Louis Bugnion, Transformation of a potline from conventional to a full flexible production unit, *Light Metals* 2019, 553-541.
2. Josh Barnes and Piet Hut, A hierarchical O(N log N) force-calculation algorithm. *Nature* volume 324, 1986, 446-449.

3. Marc Dupuis, Valdis Bojarevics and Janis Freibergs, Demonstration thermo-electric and MHD mathematical models of a 500 kA aluminum electrolysis cell: Part 2, *Light Metals* 2004, 453-459.
4. Roman Gutt, Varchasvi Nandana and Uwe Janoske, A numerical study of metal pad rolling instability in a simplified Hall-Héroult cell, *6th European Conference on Computational Mechanics (ECCM 6)*, 2018.
5. Valdis Bojarevics and Marc Dupuis, Application and adaptability of MHD stability computation for modern aluminium reduction cells at extreme conditions of low ACD, *Light Metals* 2021, 565-571.
6. Roman Düssel, *Entwicklung eines Regelungskonzepts für Aluminium-Elektrolysezellen unter Berücksichtigung einer variablen Stromstärke und eines regelbaren Wärmeverlusts*, PhD Thesis, Bergische Universität Wuppertal, Wuppertal, Germany, 2017.
7. Ron Kremser *et al.*, Comparison of different spike detection methods in Hall- Héroult cells, *Automation 2021*, Band 2392 1, Auflage 2021.